ANALYSIS OF MONO- AND MULTI-STATIC LASER RANGING SCENARIOS FOR ORBIT IMPROVEMENT OF SPACE DEBRIS

Christoph Bamann[(1)], Urs Hugentobler[(1)], Georg Kirchner[(2)], Ulrich Schreiber[(3)], Johann Eckl[(4)], and Stefan Riepl[(4)]

[(1)]*Technische Universität München, Munich, Germany*
[(2)]*Austrian Academy of Sciences, Space Research Institute, Graz, Austria*
[(3)]*Technische Universität München, Geodetic Observatory Wettzell, Germany*
[(4)]*Bundesamt für Kartographie und Geodäsie, Geodetic Observatory Wettzell, Germany*

Abstract: *The rapidly rising number of space debris objects poses an increasing threat to manned and unmanned space flight, particularly in low Earth orbits (LEOs). Increasingly important conjunction analyses and collision avoidance planning activities demand rapid and accurate orbit determination and prediction. With regard to these challenges predictions based on Two Line Elements (TLEs) tend to be too inaccurate and do not provide information about the uncertainty of the estimated orbits. However, it has recently been demonstrated that laser ranging to space debris can significantly improve the quality of orbit determination and prediction. Additionally, diffusely reflected photons from the laser in Graz have been detected in Wettzell in a bi-static laser ranging experiment. This suggests employing this technique for orbit improvement of selected objects from the TLE catalog providing additional covariance information. In this work we analyzed the potential of orbit determination based on laser ranging with particular regard to bi- and multi-static laser ranging scenarios in central Europe. To this end we selected a set of potential satellite laser ranging (SLR) stations and simulated observations using typical LEO space debris objects. Based on these we conducted covariance analyses studying the potential of conceivable mono- and multi-static laser ranging configurations. In doing so, we considered the impact of various estimation parameter sets, additional uncertain station clock synchronization, pass-station geometries and observation data rates. In its entirety this scenario analysis resulted in a concise overview of the significance of some fundamental ground system design parameters for orbit determination of space debris based on mono- and multi-static laser ranging.*

Keywords: *Space Debris, Orbit Determination, Multi-static Laser Ranging, Covariance Analysis*

1. Introduction

Space debris refers to Earth orbiting objects, which no longer serve any useful purpose. Examples are fragments resulting from collisions, break-ups and explosions, spent upper stages, and decommissioned satellites. The number of space debris objects is rising rapidly, particularly in the very populated LEO regimes, where the density of operational satellites is high. This poses an increasing threat to manned and unmanned space flight. Hence, spacecraft operators are faced with rather new challenges like conjunction analysis, collision avoidance planning and active debris removal. In this framework, reliable and accurate orbit prediction of space debris is a crucial issue. Currently, the USSTRATCOM maintains the largest space debris objects catalog with orbital information about the majority of trackable objects. This information is provided in the form of TLEs, which are mostly derived from orbit determination using radar-tracking data [1]. These TLEs are basically Kepler parameters with an additional aerodynamic drag term, which can be used for orbit prediction.

However, such predictions tend to be too inaccurate with regard to the challenges named above [2, 3]. Recently, it was shown that laser ranging to space debris targets has the potential to significantly improve the quality of orbit determination giving rise to better predictions in terms of both reliability and accuracy [4, 5]. Detecting the diffusely reflected photons of the transmitting station with several other receiving stations in multi-static ranging mode is a promising technique to further increase observability of orbit parameters with limited satellite pass durations. First results of successful experiments bi-static laser ranging to space debris are presented in [6]. Though it is not feasible to use laser ranging for maintaining a catalog of space debris objects, orbit improvement of selected objects is envisaged and expected to provide valuable support to spacecraft operations. While the above mentioned mono- and bi-static laser ranging experiments to space debris were primarily meant to study the feasibility of this technique and to test the maturity of the required technology, our results shall be useful for ground systems design to support spacecraft operations, which may require accurate orbit determination and prediction of arbitrary objects on demand.

To this end, our work focuses on the analysis of potential benefits of such multi-static tracking scenarios for orbit prediction based on laser tracking data. We study different combinations of active (transmitting) and passive (receiving) SLR stations. In doing so, first orbit determination using TLEs without uncertainty information as well as orbit refinement with information from previous object passes is considered. The presented work is based on simulated orbits and observations. Two representative space debris objects serve as the basis for covariance analyses. These facilitate an evaluation of the impact of critical system parameters like the selection of transmitting and receiving stations, station clock synchronization uncertainties and observation data rates.

The remainder of this paper is organized as follows: In section 2 we present the mathematical system formulation including the observation and dynamics models that are used for our covariance analyses. That followed, section 3 reviews some of the most relevant fundamentals of orbit determination based on batch estimation. Particular emphasis is put on covariance computation of the estimation parameters including the impact of additional uncertain parameters. In section 4 we describe our simulation setting with descriptions of the considered tracking scenarios and objects as well as the most important simulation parameters. After a discussion of our simulation results in section 5 we finish this paper with a summary and some conclusions in section 6.

2. System model

Observations in satellite laser ranging SLR are typically time-of-flight measurements of laser pulses from the transmitting station to the satellite and back. We refer to this concept as mono-static ranging, which can readily be used for ranging to space debris with some hardware modifications. With the Earth-centered-inertial position $\mathbf{X}_i(t)$ of the SLR station i we model such two-way range measurements $\tau_{ii}(t)$ for LEO objects as

$$\tau_{ii}(t) = \frac{2}{c}\left\|\mathbf{r}(t) - \mathbf{X}_i(t)\right\| + b_{a,ii} + b_{b,ii} + \nu_{ii}, \tag{1}$$

where $\mathbf{r}(t)$ denotes the position of the tracked object at the epoch of pulse reflection t noted in the same coordinate frame. In addition to the geometric range term, atmospheric delays $b_{a,ii}$ and instrumental delays $b_{b,ii}$ contribute to our time-of-flight measurement model. The measurement

noise ν_{ii} is assumed to be white Gaussian with zero-mean and constant variance σ_{ii}^2. By contrast, in a bi- or multi-static ranging scenario one station i is equipped with a transmitting laser and one or several other stations $j \neq i$ can receive the diffusely reflected laser pulses. Hence, we are potentially provided with additional time-of-flight measurements $\tau_{ij}(t)$, informally referred to as range measurements in the present work, for every remote receiving station and every transmitted laser pulse. These are modeled as

$$\tau_{ij}(t) = \frac{1}{c}\left(\left\|\mathbf{r}(t) - \mathbf{X}_i(t)\right\| + \left\|\mathbf{r}(t) - \mathbf{X}_j(t)\right\|\right) + b_{a,ij} + b_{b,ij} + b_{c,ij} + \nu_{ij} \tag{2}$$

with equivalent terms as in (1). However, the multi-static ranging model additionally incorporates the bias term $b_{c,ij}$, which accounts for the clock offset between stations i and j and may have to be estimated along with the orbital parameters of interest. Note that we regard all clock offsets $b_{c,ij}$ as constant throughout this work. Stacking all available observation data from epoch $t = t_k$ yields the measurement vector $\mathbf{y}_k$:

$$\mathbf{y}_k = \left[\tau_{11}(t_k), ..., \tau_{ij}(t_k), ..., \tau_{MN}(t_k)\right]^T + \nu_k \tag{3}$$

The scalars M and N are equal to or less than the total number of transmitting and receiving stations, respectively. As bi-static ranging is not possible in both directions at the same time, we have $\tau_{ij}(t_k) \neq \emptyset \Rightarrow \tau_{ji}(t_k) = \emptyset$. The vector ν_k contains all individual noise elements of the available observations at epoch t_k. Their corresponding variances σ_{ii}^2 and σ_{ij}^2 are combined accordingly giving the diagonal measurement noise covariance matrix Σ_k. We summarize all parameters that are required to compute $\mathbf{y}_k$ in the system state vector $\mathbf{x}(t)$. This vector comprises the parameters that completely describe the object's orbit as well as potentially unknown observation parameters such as as the constant station clock offsets. More specifically, we model the object dynamics using simple two-body gravitational acceleration. Such orbits are fully described by Kepler parameters, implying that position and velocity are determined for all times if they are determined for a single reference epoch $t = t_*$. Consequently, with the vector of all bi-static station clock offsets $\mathbf{b}_c$ the full system model can concisely be stated as

$$\mathbf{y}_k = \mathbf{h}_k(\mathbf{x}_*) + \nu_k \quad \text{with} \quad \mathbf{x}_* = \mathbf{x}(t_*) = \left[\mathbf{r}(t_*)^T, \mathbf{v}(t_*)^T, \mathbf{b}_c^T\right]^T. \tag{4}$$

3. Batch estimation and covariance computation

Based on (4) and the set of true observation data $\tilde{\mathbf{y}}_k$ a batch filter iteratively adjusts the estimate $\hat{\mathbf{x}}_*$ of the true state $\mathbf{x}_*$ so as to minimize the cost function

$$\sum_k \mathbf{W}_k\left(\tilde{\mathbf{y}}_k - \mathbf{h}_k(\hat{\mathbf{x}}_*)\right)^2 + \mathbf{W}_*\left(\hat{\mathbf{x}}_* - \hat{\mathbf{x}}_*^-\right)^2, \tag{5}$$

where $\hat{\mathbf{x}}_*^-$ is the a-priori state estimate with covariance matrix $\hat{\mathbf{P}}_*^- = \mathbf{E}\{(\hat{\mathbf{x}}_*^- - \mathbf{x}_*)(\hat{\mathbf{x}}_*^- - \mathbf{x}_*)^T\}$ and the weight matrices $\mathbf{W}_k = \Sigma_k^{-1}$, $\mathbf{W}_* = \hat{\mathbf{P}}_*^-$ denote the observation weight and a-priori information matrices, respectively. The minimization is performed via iterative Gauss-Newton optimization starting with $\hat{\mathbf{x}}_*^{(0)} = \hat{\mathbf{x}}_*^-$:

$$\hat{\mathbf{x}}_*^{(i)} = \hat{\mathbf{x}}_*^{(i-1)} + \Delta\hat{\mathbf{x}}_*^{(i)} \tag{6}$$

$$\Delta\hat{\mathbf{x}}_*^{(i)} = \left(\mathbf{W}_* + \sum_k \mathbf{A}_k^T(\hat{\mathbf{x}}_*^{(i-1)}) \mathbf{W}_k \mathbf{A}_k(\hat{\mathbf{x}}_*^{(i-1)}) \right)^{-1} \sum_k \mathbf{A}_k^T(\hat{\mathbf{x}}_*^{(i-1)}) \mathbf{W}_k (\tilde{\mathbf{y}}_k - \mathbf{y}_k) \tag{7}$$

The matrix $\mathbf{A}_k$ represents the sensitivity of the observations $\mathbf{y}_k$ with respect to $\mathbf{x}_*$, i.e. $\mathbf{A}_k(\mathbf{x}_*) = \partial \mathbf{h}_k(\mathbf{x}_*)/\partial \mathbf{x}_*$. Based on the converged least-squares state estimate $\hat{\mathbf{x}}_*$ the a-posteriori covariance matrix $\hat{\mathbf{P}}_* = \mathbf{E}\{(\hat{\mathbf{x}}_* - \mathbf{x}_*)(\hat{\mathbf{x}}_* - \mathbf{x}_*)^T\}$ is given by

$$\hat{\mathbf{P}}_* = \left(\mathbf{W}_* + \sum_k \mathbf{A}_k^T(\hat{\mathbf{x}}_*) \mathbf{W}_k \mathbf{A}_k(\hat{\mathbf{x}}_*) \right)^{-1} . \tag{8}$$

If not the whole state vector $\mathbf{x}_*$ shall be estimated due to uncertain knowledge of some of its elements, it can be divided into a solve-for part $\mathbf{x}_*^s$ and a consider part $\mathbf{x}_*^c$. While $\mathbf{x}_*^s$ contains all elements that shall be estimated in the least squares adjustment, $\mathbf{x}_*^c$ contains the known but uncertain elements with covariance matrix Σ^{cc} that shall not be estimated. Consider-covariance analyses account for the impact of the uncertainty Σ^{cc} on the solve-for state estimation covariance by determining how Σ^{cc} enters the solution through least squares adjustment. To deliver some insight into the mathematics we first rewrite the observation model (4) such that it takes the form

$$\mathbf{y}_k = \mathbf{h}_k(\mathbf{x}_*^s, \mathbf{x}_*^c) + \nu_k. \tag{9}$$

With the partial derivatives $\mathbf{A}_k^s$ and $\mathbf{A}_k^c$ of the modeled measurements $\mathbf{y}_k$ with respect to $\mathbf{x}_*^s$ and $\mathbf{x}_*^c$, respectively, we linearize expression (9) about a reference state to yield the differential relation

$$\Delta\mathbf{y}_k = \mathbf{A}_k^s \Delta\mathbf{x}_*^s + \mathbf{A}_k^c \Delta\mathbf{x}_*^c + \nu_k. \tag{10}$$

This relation shows how variations of the observations with the solve-for parameters are not only affected by measurement noise but also by the term $\mathbf{A}_k^c \Delta\mathbf{x}_*^c$, where $\Delta\mathbf{x}_*^c$ is a random variable with zero-mean and covariance matrix Σ^{cc}. Assuming that $\Delta\mathbf{x}_*^c$ and ν_k are uncorrelated it is straightforward to derive

$$\hat{\mathbf{P}}_*^{sc} = \hat{\mathbf{P}}_*^{ss} + \hat{\mathbf{P}}_*^{cc} = \hat{\mathbf{P}}_*^{ss} + \left(\hat{\mathbf{P}}_*^{ss} \sum_k \mathbf{A}_k^{sT} \mathbf{W}_k \right) \left(\sum_k \mathbf{A}_k^c \Sigma^{cc} \mathbf{A}_k^{cT} \right) \left(\hat{\mathbf{P}}_*^{ss} \sum_k \mathbf{A}^{sT} \mathbf{W}_k \right)^T . \tag{11}$$

The conventional measurement noise related covariance matrix $\hat{\mathbf{P}}_*^{ss}$ is computed as in Eq. (8). Together with the additional contribution from the uncertain consider parameters $\hat{\mathbf{P}}_*^{cc}$ it yields the total covariance matrix $\hat{\mathbf{P}}_*^{sc}$. While the impact of observation noise is essentially averaged out and the uncertainty $\hat{\mathbf{P}}_*^{ss}$ of the estimated parameters is decreased with an increasing number of measurements, the matrix $\hat{\mathbf{P}}_*^{cc}$ must be interpreted differently. The consider parameters are assumed to be known with a given uncertainty Σ^{cc}, which is mapped into a corresponding uncertainty of the estimated parameters and does not decrease with increasing data rate, but is essentially constant for a given data arc and tracking configuration. Therefore, it is well suited to assess the impact of systematic errors in the orbit determination. In the present work such consider parameters are the station clock offsets, which are crucial in bi- and multi-static laser ranging scenarios. See, for example, [7, 8] for more details about (consider) covariance analyses.

In Cartesian coordinate representation the diagonal elements of the covariance matrix $\hat{\mathbf{P}}$, which might represent $\hat{\mathbf{P}}_*$ or $\hat{\mathbf{P}}_*^{sc}$, are designated as $\mathrm{diag}[\hat{\mathbf{P}}] = [\sigma_{r_x}^2, \sigma_{r_y}^2, \sigma_{r_z}^2, \sigma_{v_x}^2, \sigma_{v_y}^2, \sigma_{v_z}^2, \sigma_{b_{c,12}}^2, \ldots, \sigma_{b_{c,MN}}^2]$.

Note that not all of the elements related to clock offsets might be present due to the considered solve-for parameter set. To assess the scenario dependent orbit determination quality we define the estimation uncertainties of position σ_r, velocity σ_v and station clock offsets σ_{b_c} as follows:

$$\sigma_r = \sqrt{\sigma_{r_x}^2 + \sigma_{r_y}^2 + \sigma_{r_z}^2}, \quad \sigma_v = \sqrt{\sigma_{v_x}^2 + \sigma_{v_y}^2 + \sigma_{v_z}^2}, \quad \sigma_{b_c} = \sqrt{\sum_{i \neq j} \sigma_{b_{c,ij}}^2} \tag{12}$$

Position and velocity uncertainties σ_r and σ_v behave consistently in all of our simulations since the position states are linked to the velocity states by an integration through the system dynamics model. Hence, to present our results we focus on σ_r for clarity.

4. Simulation setting

In this section we introduce the considered tracking scenarios and related baseline parameters. We present the selected space debris objects including tracking schedules and ground tracks resulting from 24-hour orbit simulations. Finally, estimator related issues namely a-priori information and estimation parameters are addressed.

4.1. Tracking scenarios and parameters

Amongst others, possible SLR stations with common-view possibility for LEO debris are Wettzell, Graz, Zimmerwald and Potsdam. We explicitly analyze the possibility of considering receive-only telescopes to improve orbit determination accuracy without the costs of operating additional active lasers. For our specific multi-static tracking scenario analyses we select a set of four stations in central Europe (see Tab. 1, left). Our considered set of scenarios is presented by Tab. 1 (right).

Station ID	Station location
(1)	Wettzell
(2)	Graz
(3)	Zimmerwald
(4)	Potsdam

Scenario ID	Tx stations	Rx stations
1	(1)	(1)
2	(1)	(1), (2)
3	(1)	(1), (2), (3)
4	(1)	(1), (2), (3), (4)
5	(1), (2)	(1), (2) mono
6	(1), (2)	(1), (2)
7	(1), (2)	(1), (2), (3)
8	(1), (2)	(1), (2), (3), (4)

Table 1: Selected set of SLR stations (left) and considered mono-, bi- and multi-static laser ranging scenarios (right). Note that scenario 5 includes only mono-static ranging and bi-static ranging between Wettzell and Graz is simulated in only one direction in scenarios 6 to 8.

Unless stated otherwise all simulations are based on the same baseline parameter set, which is summarized by Tab. 2. In view of the experiments [4] and [9] our assumed measurement noise variances $\sigma_{ii} = \sigma_{ij} = 1$ m accounting for non-systematic errors are rather conservative (the cited references report values of 0.7 m and 0.6-0.8 m, respectively). Moreover, very conservative data rates of 0.1 Hz are assumed in view of data filtering under potentially adverse noise conditions. These may result from partially clouded skies or long detector activation times as a consequence of imprecise

Parameter	Value
Mono-static observation data rate f_{ii}	0.1 Hz
Bi- and multi-static observation data rate f_{ij}	0.1 Hz
Mono-static measurement noise uncertainty σ_{ii}	1 m
Bi-and multi-static measurement noise uncertainty σ_{ij}	1 m

Table 2: Baseline simulation parameters.

a-priori orbits from TLE data. This holds particularly for bi- and multi-static ranging as activation times of the single photon detectors must be even longer in presence of clock synchronization errors.

4.2. Space debris object selection

Our chosen objects shall be representative for the spatial density distribution of space debris. Peaks of high density exist in circular LEOs with altitudes between 800 km and 1000 km and characteristic high inclinations [10]. Timely constraints arise from tracking requests for orbit refinement of a space debris object in case of a critical conjunction warning. In such cases only up to 48 hours are available for radar tracking campaigns [11]. This motivates the restriction of our simulations to 48 hour intervals. In view of the myriad of conceivable parameter combination for the scenario analyses, we consider only two space debris objects with nearly identical orbit geometries. Both objects represent typical LEO objects with an altitude of approximately 800 km in near-circular orbits. To obtain distinctively different passes, the orbits of the chosen objects have inclinations of $\sim 98^\circ$ (object 1) and $\sim 50^\circ$ (object 2). Simulated visibility times of these two objects for the selected ground stations as well as the ground tracks during these visibility times are illustrated by Fig. 1 and Fig. 2, respectively. The colors of the ground tracks (reddish and blueish) are used throughout the presentation of our simulation results in section 5 to clarify to which object we refer.

4.3. A-priori information and estimation parameters

All orbit determination algorithms require an initial estimate of the state vector, which is commonly obtained by performing an initial orbit determination (IOD) step. This estimate is commonly improved by batch estimation taking a whole set of available observations into account (see section 3). However, to track space debris with a typical SLR telescope a-priori orbit information is already required to find the object given the telescope's small field-of-view. We obtain this information from the cataloged and readily available TLEs as mentioned in the introduction. These TLEs can be propagated to the required epoch, transformed to topocentric coordinates, and eventually acquired on the sky. Hence, the opportunity to use TLE data for initializing the batch estimation algorithm renders the typical IOD methods unnecessary. Due to the lack of reliable information about the uncertainty in the TLE data, we assume zero a-priori information $\mathbf{W}_* = (\hat{\mathbf{P}}_*^-)^{-1} = \mathbf{0}$.

As spacecraft operators often require the total amount of orbit information to be collected rapidly, it may only be feasible to estimate a few parameters such as the Kepler elements. However, using merely single pass observation data it might even be impossible to estimate these six parameters

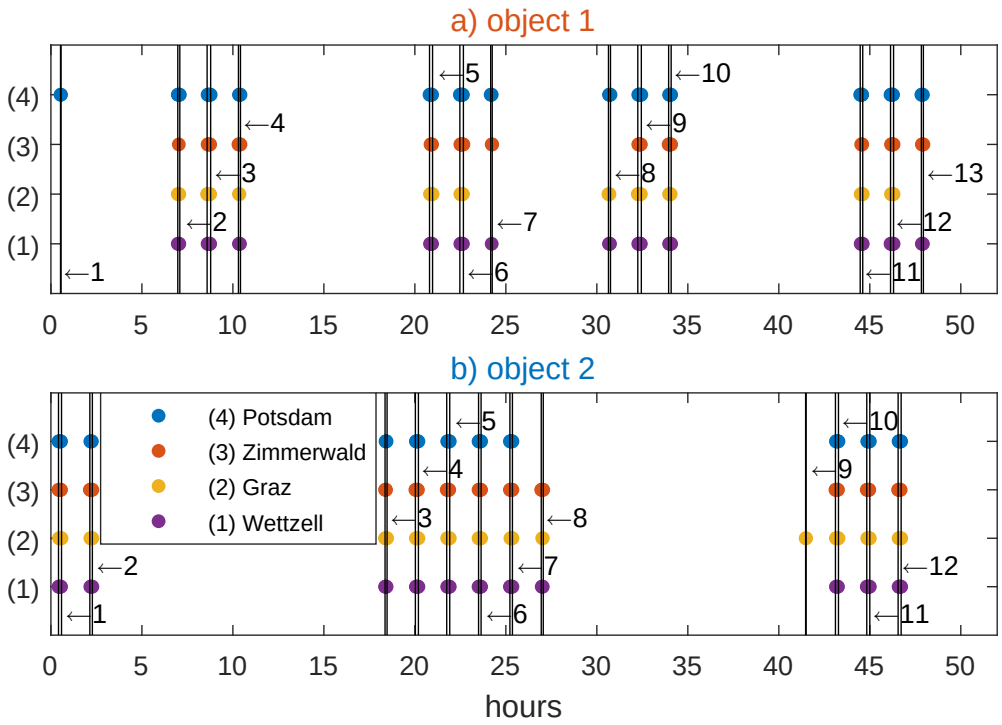

Figure 1: Passes during which the objects are visible for at least one of the four listed tracking stations in a 48-hour simulation: Near-circular LEO objects at approximate heights of ∼800 km and inclinations of a) ∼ 98° (object 1) and b) ∼ 50° (object 2).

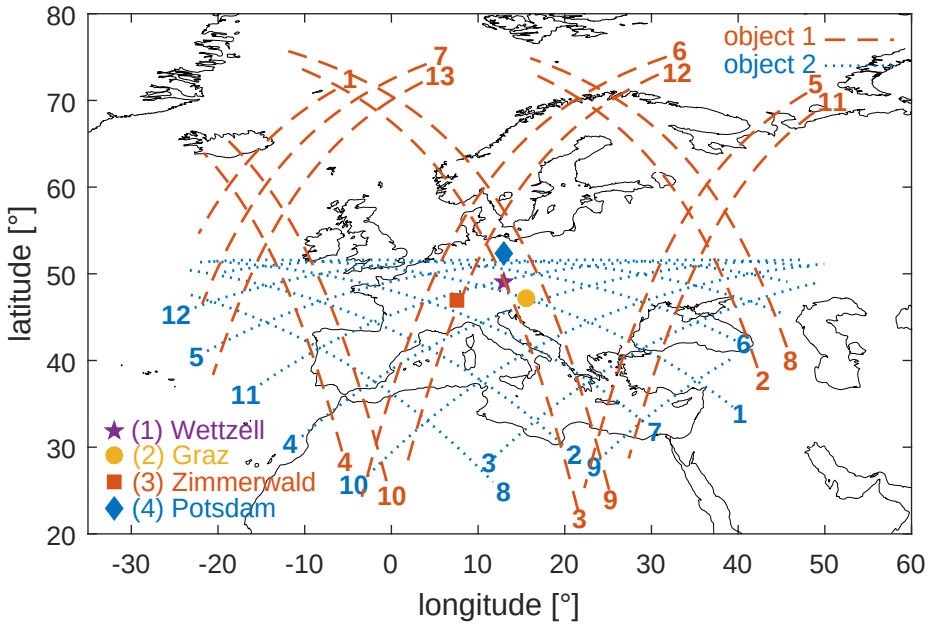

Figure 2: Ground tracks of the two considered near-circular LEO objects as in Fig. 1 a) (object 1,red) and b) (object 2,blue). The ground tracks are only plotted whenever the objects are visible for at least one ground station. The pass numbers are shown as indicated by Fig. 1.

depending on the scenario-pass geometry and other system parameters. Such problems can potentially be overcome by estimating four-parameter subsets based on the assumption of circular orbits. Moreover, one relevant challenge of bi- and multi-static tracking scenarios is clock synchronization between the participating stations, which directly affects the ranging observations. Therefore, these observation model parameters can either be regarded as uncertain consider parameters with covariance matrix $\mathrm{diag}[\Sigma^{cc}] = [\sigma_{b_{c,12}}, ..., \sigma_{b_{c,ij}}, ..., \sigma_{b_{c,MN}}]$ with $i \neq j$ (see Eq. (11)). Alternatively, they can be estimated as part of an extended solve-for state vector, which further complicates the data-starved problem. In doing so, we always assume constant offsets across all passes.

5. Simulation results

First this section presents simulation results based on single pass observations. These deliver insight into fundamental characteristics of the new observation types of bi- and multi-static laser ranging by relating estimation parameter uncertainty to scenario-pass geometry. They further serve as a basis for interpreting the results of covariance analyses based on multiple pass observation data, which is presented in the second part of this section.

5.1. Single pass observations

According to [12], a nonlinear time-varying system is locally observable if its observability Gramian $\mathscr{O}$ is full rank, i.e. $\mathrm{rank}(\mathscr{O})$ is equal to the number of solve-for parameters. Observability implies that it is possible to estimate all solve-for parameters given a certain set of observations. For the considered system, $\mathscr{O}$ is defined as

$$\mathscr{O} = \sum_k \mathbf{A}_k^T \mathbf{W}_k \mathbf{A}_k, \tag{13}$$

which is the inverse of the covariance matrix without a priori information (see Eq. (8)). The observability of the estimation parameters based on single pass observations is illustrated by Fig. 3, which further contains the number of simulated observations per scenario-pass combination. More receiving stations do not always yield more observations due to visibility constraints. Pass 1 of object 1 is in fact visible for the station in Potsdam, but there are no observations as it is not visible for any of the transmitting stations (Wettzell, Graz) in the considered scenarios. As the number of solve-for parameters increases, less scenario-pass combinations prove to be suited for obtaining first estimates of these parameters. For example, while Kepler orbit determination with only one mono-static ranging station is always impossible, all of the six orbital parameters can be estimated using data of most passes once additional bi-static ranging is considered. If the solve-for parameter set is further extended by station clock offsets, several additional scenario-pass combinations become unobservable. This is due to the fact that the very short-arc observation data yields too strong correlations between station clock offsets and orbital elements rendering estimation of either parameters impossible.

Considering the simulated values of σ_r for estimated Kepler orbits assuming perfectly synchronized clocks and estimated Kepler orbits plus clock offsets individually, the benefit of multi-static tracking becomes even more evident. The position uncertainty decreases with increasing number of receiving stations (scenarios 2-4) as Fig. 4 shows. This effect is even stronger if a second transmitting station

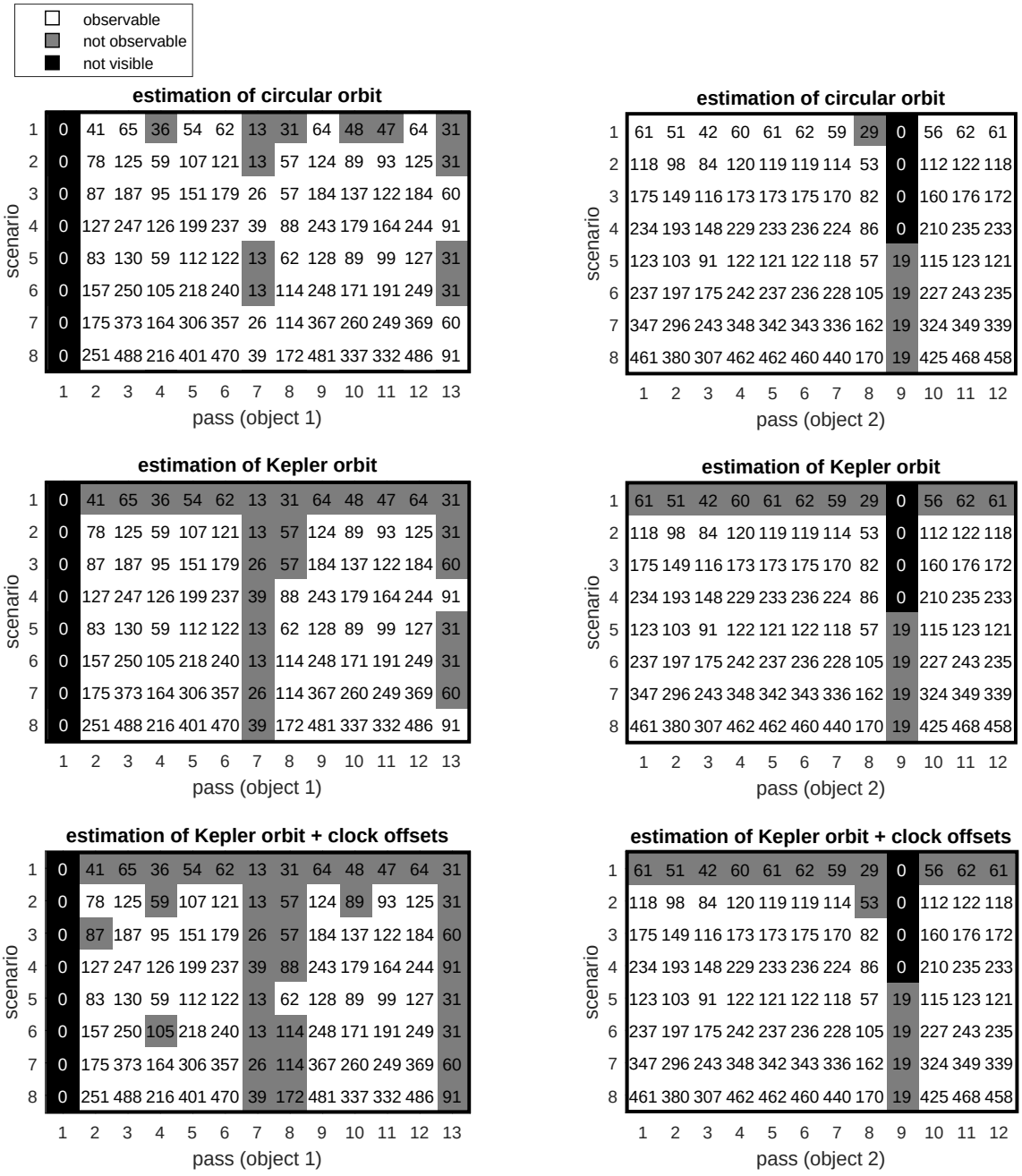

Figure 3: Observability of all scenario-pass combinations of object 1 (left) and object 2 (right) based on single pass data. The numerical values in the matrices indicate the number of available observations for each combination.

is considered (scenarios 5-8). Moreover, σ_r depends highly on the respective passes. Comparison with Fig. 2 reveals that passes, during which the observation geometry changes significantly, provide much more information about the system parameters than passes, where the objects attain only low elevations. In the latter case, estimating unknown clock offsets considerably worsens the situation or makes estimation impossible due to the aforementioned correlations. Generally, σ_r is notably smaller for object 2 than for object 1. This is due to better observation geometries as the inclination of object 2 is within the range of the station latitudes.

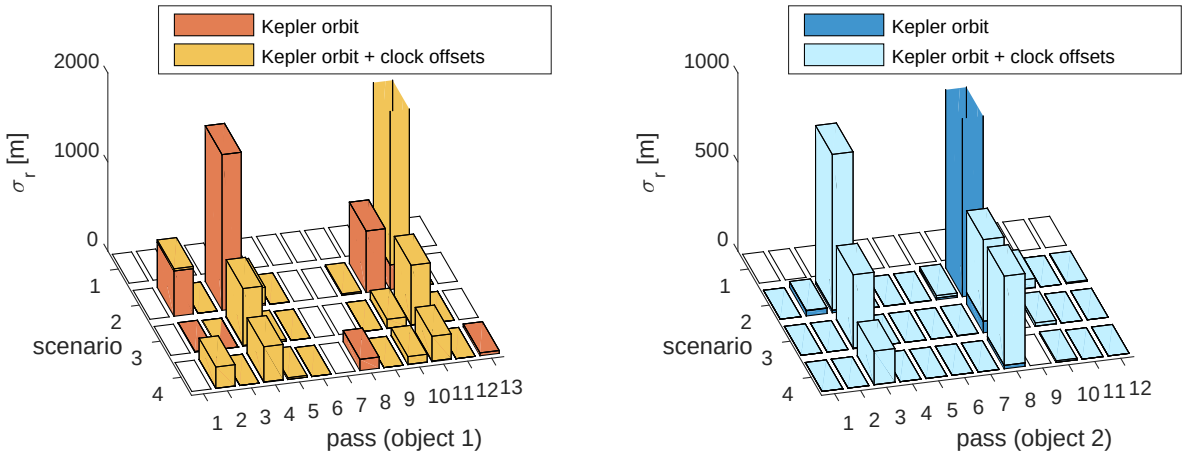

Figure 4: Position uncertainties for different solve-for parameter sets and no consider parameters. Light colors show how much uncertainty additional estimation of clock offsets adds to the position uncertainty of sole Kepler orbits. Missing bars indicate that a parameter set is not observable.

Instead of estimating the clock offsets based on observation data, they can be assumed known from other synchronization techniques with some uncertainty. Consider-covariance analyses take this uncertainty into account to provide more realistic and meaningful orbit determination uncertainties in such cases. Clock offset uncertainty of $\sigma_{b_{c,ij}} = 1$ ns has almost no impact on the solution as Fig. 5 (top row) shows. This is plausible in view of the assumed laser ranging measurement noise of $\sigma_{ii} = \sigma_{ij} = 1$ m as light travels about 30 cm in 1 ns. By contrast, Fig. 5 (bottom row) reveals how clock synchronization uncertainty of $\sigma_{b_{c,ij}} = 10$ ns, corresponding to approximately 3 m travel distance of a laser pulse, degrades the single pass solutions. Moreover, it becomes apparent that the additional uncertainty due to the consider parameters scales with the uncertainty due to measurement noise only (see Eq. (11)).

Just as the effects of considering uncertain clock offsets, the effects of bi- and multi-static observation data rates on σ_r depend highly on the observation geometry as Fig. 6 shows. This becomes evident in view of Eq. (8), where the number of observations indeed affects the number of summation terms but the corresponding sensitivity matrices $\mathbf{A}_k$ stay practically unchanged. In view of technical system limitations the effect is clearly less critical as compared to variations in the consider parameters $b_{c,ij}$. Anyway, both clock synchronization and observation data rates are linked by the fact that better clock synchronization facilitates shorter detector activation gates in single photon detection mode, which in turn support higher signal-to-noise ratios.

5.2. Multiple pass observations

When considering multiple pass observations we are particularly interested in the amount of uncertainty that is added to Kepler orbit estimation by either considering the clock offsets as uncertain parameters or estimating them based on observation data. In this context, Fig. 7 presents some interesting results. Conditions are shown, under which adding further stations with consider variance $\sigma_{b_{c,ij}} = 10$ ns (Fig. 7, middle column) even degrades the orbit determination performance. For these passes some bi-static ranges are very sensitive to the solve-for parameters so that these

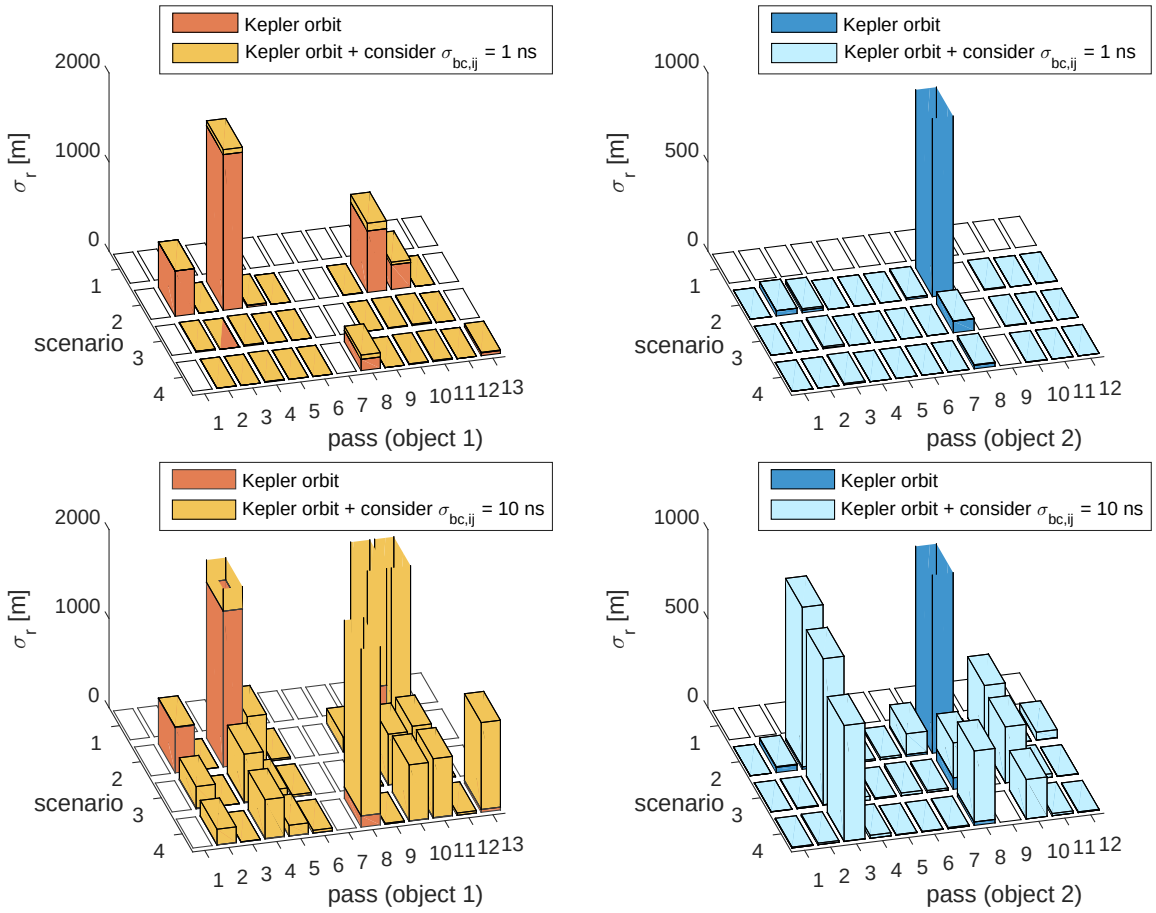

Figure 5: Kepler orbit estimation with and without considering uncertain station clock offsets. The light colors indicate how much uncertainty the uncertain station clock offsets add to σ_r of the sole Kepler parameter estimation.

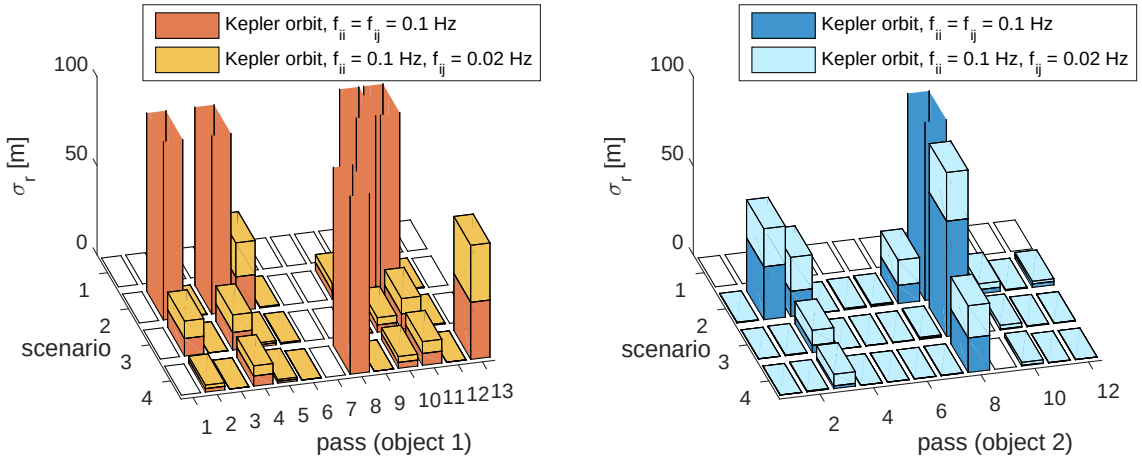

Figure 6: Kepler orbit estimation using different bi- and multi-static observation data rates. The light colors indicate how much uncertainty the lower observation data rates add to σ_r of the baseline scenario (see Tab. 2).

observations enter the solution with high relative weight. However, their uncertainty is actually larger than the assumed observation noise. Fig. 7 (right column) shows the uncertainty that is added by additionally estimating the station clock offsets. While σ_r highly depends on the respective scenarios using data from the first pass only, almost no further uncertainty is added to the Kepler orbit solution if observation data from a further pass obtained. This implies that the additional observation data is suited to efficiently decorrelate the clock offset estimates from the orbital parameters. Note that pass 9 of object 2 is not visible for the station in Wettzell leaving the uncertainties for scenarios 1 to 4 unaffected.

In conclusion, orbit determination with accurate station synchronization (σ_{ij} =1 ns) is mostly superior to clock offset estimation in multi-static ranging scenarios with observation data from only one pass. However, our results also reveal that uncertain clock synchronization can significantly corrupt orbit determination if the uncertainty exceeds the measurement noise, also in case of observation data from multiple passes. Moreover, clock offset estimation does not pose a problem anymore, if data from multiple passes is considered.

6. Conclusion

This paper presented simulations, which deliver general insights into potential benefits and challenges of mono- and multi-static laser ranging scenarios for orbit improvement of space debris. Our simulations consistently demonstrated that adding further receiving stations is suited to reduce estimation parameter uncertainty. We illustrated that, after only one pass, the observability Gramian tends to be singular due to poor tracking geometries. These result in a set of observations, which are not very sensitive to the estimation parameters. It could be demonstrated that assuming circular orbits may allow determination of the remaining four Kepler elements in such cases. Under certain conditions this was even possible with mono-static range measurements from a single pass only. In addition, we found that distinctly lower multi-static observation data rates are potentially less detrimental than uncertain clock synchronization. Therefore, the problem of station clock synchronization was discussed and the effects of using known but uncertain clock offsets were compared with the effects of estimating clock offsets based on observation data. While the former approach provided good results in case of small synchronization uncertainties in the range of the measurement noise, increasing these uncertainties by one order of magnitude was shown to significantly degrade the orbit solutions. Estimating clock offsets might also introduce much uncertainty in presence of single pass observation data only, but consistently performs well once additional data from a second pass is obtained. In this regard correlations between clock offsets and orbit parameters were reduced considerably in our simulations. Hence, incorporating them into the estimation parameter set added almost no additional uncertainty to the estimated orbit parameters.

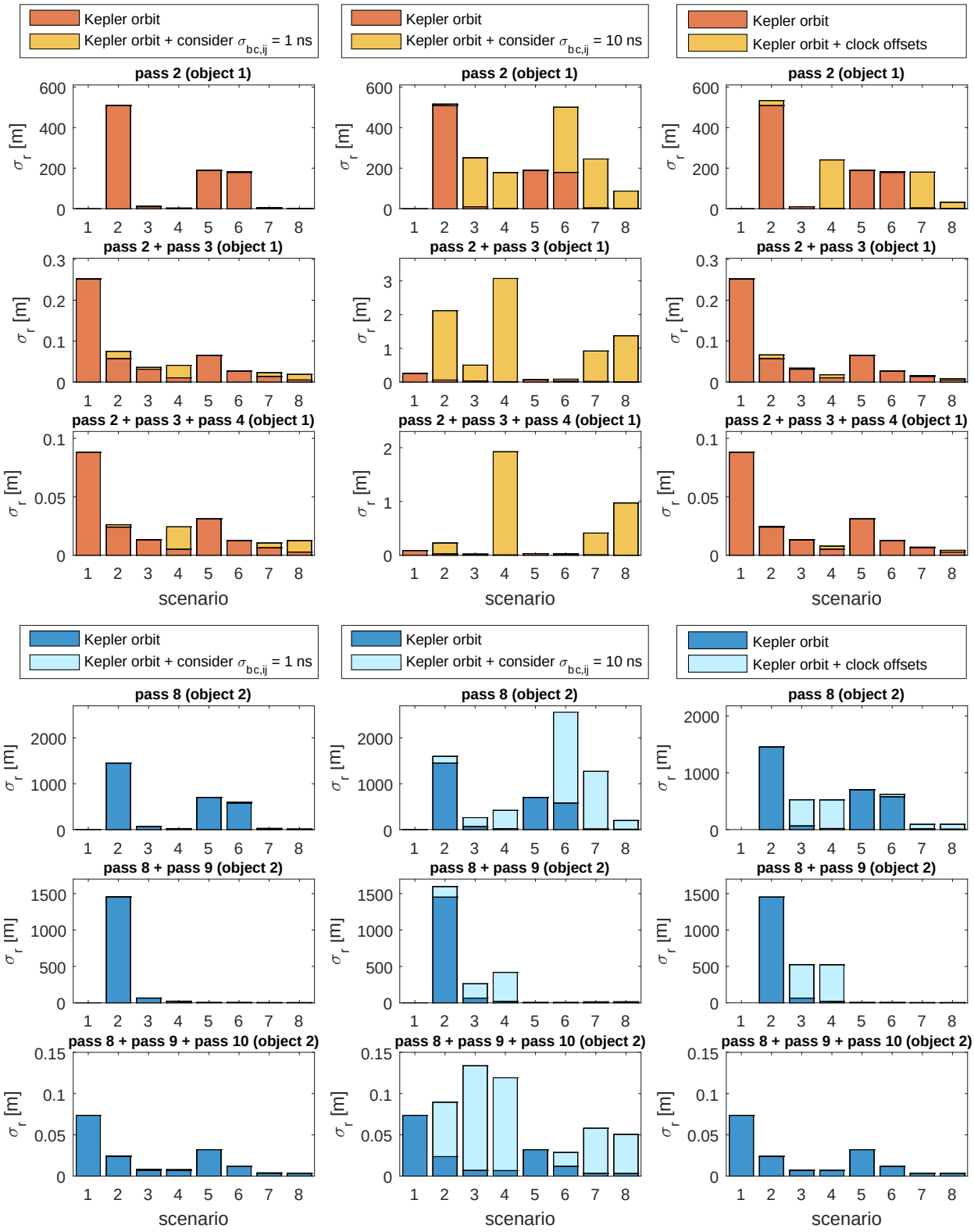

Figure 7: Orbit determination uncertainties σ_r with observation data from one, two or three consecutive passes considering not estimated but uncertain (left and middle) and estimated (right) clock offsets.

7. References

[1] Vallado, D. A., Crawford, P., Hujsak, R., and Kelso, T. "Revisiting spacetrack report #3." Proceedings of the 2006 AIAA/AAS Astrodynamics Specialist Conference, 2006.

[2] Wang, R., Liu, J., and Zhang, Q. "Propagation errors analysis of TLE data." Advances in Space Research, Vol. 43, No. 7, 2009.

[3] Flohrer, T., Krag, H., and Klinkrad, H. "Assessment and categorization of TLE orbit errors for the US SSN catalogue." Advanced Maui Optical and Space Surveillance Technologies Conference (AMOS), 2008.

[4] Kirchner, G., Koidl, F., Friederich, F., Buske, I., Völker, U., and Riede, W. "Laser measurements to space debris from Graz SLR station." Advances in Space Research, Vol. 51, No. 1, 2013.

[5] Baur, O., Wirnsberger, H., Kirchner, G., Schreiber, K. U., and Riede, W. "On the potential of multi-static SLR. Case study: orbit determination and prediction of space debris objects." AGU Fall Meeting Abstracts, Vol. 1, 2014.

[6] Wirnsberger, H., Baur, O., and Kirchner, G. "Space debris orbit prediction errors using bi-static laser observations. Case study: ENVISAT." Advances in Space Research, 2015.

[7] Montenbruck, O. and Gill, E. Satellite orbits: models, methods and applications. Springer Science & Business Media, 2012.

[8] Markley, F. L. and Carpenter, J. R. "Generalized Linear Covariance Analysis." The Journal of the Astronautical Sciences, Vol. 57, No. 1-2, 2009.

[9] Zhang, Z.-P., Yang, F.-M., Zhang, H.-F., Wu, Z.-B., Chen, J.-P., Li, P., and Meng, W.-D. "The use of laser ranging to measure space debris." Research in Astronomy and Astrophysics, Vol. 12, No. 2, 2012.

[10] Klinkrad, H. Space debris. Wiley Online Library, 2010.

[11] Aida, S. and Kirschner, M. "Collision risk assessment and operational experiences for LEO satellites at GSOC." Journal of Aerospace Engineering, Vol. 4, No. 2, 2012.

[12] Huxel, P. J. and Bishop, R. H. "Navigation algorithms and observability analysis for formation flying missions." Journal of guidance, control, and dynamics, Vol. 32, No. 4, 2009.